J Mater Sci (2018) 53:2697–2708

Energy materials

In situ synthesis of $Fe_{(1-x)}Co_xF_3$/MWCNT nanocomposites with excellent electrochemical performance for lithium-ion batteries

Jun Li[1,*], Shuaijun Xu[1], Si Huang[1], Lu Lu[1], Lifang Lan[1], and Shaofang Li[1]

[1] *Faculty of Chemical Engineering and Light Industry, Guangdong University of Technology, No. 100 Waihuan Xi Road, Guangzhou Higher Education Mega Center, Panyu District, Guangzhou, Guangdong 510006, China*

Received: 12 August 2017
Accepted: 5 October 2017
Published online: 13 October 2017

ABSTRACT

Due to their high theoretical capacities and high energy densities, metal fluorides have attracted significant attention as cathodes for lithium-ion batteries. However, thus far, their low conductivities have limited the performance of these materials. In this work, the $Fe_{(1-x)}Co_xF_3$/MWCNT (multi-walled carbon nanotube) nanocomposites ($x = 0$, 0.02, 0.04 and 0.06) are obtained by an in situ solvothermal method with Co-doping and wrapping of the MWCNTs. The results indicate that Co-doping can adjust the crystal structure, decrease the band gaps and enhance the Li^+ diffusion coefficient of FeF_3. Additionally, the wrapped network of MWCNTs enhances the conductivity of the composites and improves their electrochemical performances. The $Fe_{0.96}Co_{0.04}F_3$/MWCNT nanocomposites exhibit a high initial discharge capacity of 217.0 mAh g^{-1} at rate of 0.2 C within the potential range of 2.0–4.5 V, which is much higher than that of the FeF_3/MWCNT counterpart (192.1 mAh g^{-1}). The discharge capacities of these two samples remain at 187.9 and 160.7 mAh g^{-1} even after 50 cycles. Meanwhile, the EIS results reveal that both the Li^+ charge transfer resistance ($R_{ct} = 31.25\ \Omega$) and Li^+ diffusion coefficient (1.40×10^{-11} cm^2 s^{-1}) are satisfactory from Co-doping and the in situ wrapping of the MWCNTs.

Introduction

With developments in science and technology, the demand for energy is increasingly growing. Lithium-ion batteries (LIBs) have attracted significant attention because of their low cost, low toxicity and sustainable development [1, 2]. FeF_3 has attracted considerable attention as an LIBs cathode due to the advantages of a high theoretical capacity (about 712 mAh g^{-1} in the voltage range of 1.0–4.5 V and 237 mAh g^{-1} in the range of 2.0–4.5 V), high energy density (~1950 Wh kg^{-1}) and good thermal stability [3–5]. Despite these overwhelming advantages, this material still cannot be applied in industry due to the intrinsically slow ionic diffusion and poor conductivity of the fluoride species [6, 7].

Address correspondence to E-mail: qhxylijun@gdut.edu.cn

DOI 10.1007/s10853-017-1685-2

To improve the electrochemical performance of FeF_3, many methods have been developed, such as creating composites with conductive agents and expanding the crystal structure [8]. The addition of carbon black [9], carbon nanotubes [10], graphene [11, 12] or V_2O_5 [13] through mechanical ball milling results in FeF_3 composites with better electrochemical performances than pure FeF_3. The uniform distribution of conductive agents in the composite will benefit the electronic conductivities. Open structures of FeF_3, *i.e.*, hexagonal tungsten bronze-type FeF_3·$0.33H_2O$ [14, 15], pyrochlore-type $FeF_3{\cdot}0.5H_2O$ [10, 16] and metal-doped FeF_3, can substantially improve the performance of this material [10, 18, 19]. Structural expansion of fluorides can increase ionic conductivities, which has been proved by researchers [8].

In this study, we utilized a solvothermal method and heat treatment to synthesize high-performance $Fe_{(1-x)}Co_xF_3$/MWCNTs (multi-walled carbon nanotubes). Since the CoF_3 and FeF_3 exhibit similar structures and electrochemical properties as the cathode materials in LIBs, the replacement of one Fe atom by a Co atom may have a better performance [17]. It has been found that a suitable Co-doped can slightly distort the crystal structure and still remain structure stable of FeF_3 [18]. Additionally, we researched the performances and electronic structures of Co-doped FeF_3 with a ReO_3-type structure through XRD phase analysis and first-principles methods [19]. It has also been proved that a suitable Co-doped can decrease the band gaps of FeF_3 and effectively improve the conductivity of FeF_3 [20]. Moreover, through the combination of wrapping with the MWCNTs and Co-doping, the as-prepared $Fe_{(1-x)}Co_xF_3$/MWCNTs showed remarkably improved electrochemical properties. The in situ wrapped MWCNTs not only could homogeneously and intimately contact with $Fe_{(1-x)}Co_xF_3$ particles, but also improved the particle size distribution. The physicochemical and electrochemical performances of the $Fe_{(1-x)}Co_xF_3$/MWCNT nanocomposites were studied in detail.

Experimental

Synthesis of $Fe_{(1-x)}Co_xF_3$/MWCNT nanocomposites

$Fe_{(1-x)}Co_xF_3$/MWCNT nanocomposites ($x = 0$, 0.02, 0.04 and 0.06) were synthesized by a solvothermal method. First, 12.12 g of iron(III) nitrate nonahydrate ($Fe(NO_3)_3{\cdot}9H_2O$) and cobalt(III) oxide (Co_2O_3) in molar ratios of 1:0, 0.98:0.01, 0.96:0.02 and 0.94:0.03 were homogeneously dissolved in anhydrous ethanol to obtain solutions. Next, 0.2 mL of Tween 80 and the MWCNTs ($Fe_{(1-x)}Co_xF_3$: MWCNTs = 0.99:0.01, 0.97:0.03, 0.95:0.05 by weight) were added to the solutions. After the solutions were stirred for 10 min, 12 mL of HF (40 wt%) was added, and the mixtures were transferred to sealed Teflon containers and ultrasonicated for 5 min to form uniform mixtures. Second, the containers were dried at 120 °C under vacuum for 6 h until precipitate was obtained. Then, the precipitates were washed with anhydrous ethanol several times and dried in an oven at 80 °C for 4 h. Finally, the precipitates were calcined at 240 °C for 3 h in a tube furnace under Ar flow (40 sccm), and after high-energy ball milling for 3 h, the $Fe_{(1-x)}Co_xF_3$/MWCNT nanocomposites were obtained.

Materials characterization

The crystal structures of the samples were characterized by X-ray diffraction (XRD) patterns on a Bruker D8 Advance diffractometer using Cu Kα radiation. The morphologies of samples were obtained by scanning electron microscopy (SEM, JEOL JMS-6700F) with energy-dispersive spectroscopy (EDS) and transmission electron microscopy (TEM, JEOL JEM-2010).

The working electrodes were composed of the $Fe_{(1-x)}Co_xF_3$/MWCNT nanocomposites and polyvinylidene fluoride (PVDF) as a binder at a weight ratio of 95:5 in *N*-methylpyrrolidone (NMP, Aldrich). Then, each slurry was evenly coated on aluminum foil. Afterward, the electrodes were dried in a vacuum oven at 85 °C for 4 h. A solution of 1 M $LiPF_6$ dissolved in a mixture of ethylene carbonate-dimethyl carbonate-ethyl methyl carbonate (EC-DMC-EMC; 1:1:1, volume ratio) was used as the electrolyte. Coin-type cells (CR2032) were assembled in an Ar-filled glove box with lithium foil as the negative electrode and Celgard 2400 as a separator. The amounts of

carbon and cobalt in the samples were verified by elemental analysis (CHNS E.A.).

Electrochemical measurements

Galvanostatic charge–discharge tests were conducted using a Neware CT3008W instrument over a voltage a range from 2.0 to 4.5 V at 25 °C. Cyclic voltammetry (CV) and electrochemical impedance spectroscopy (EIS) were performed with an electrochemical workstation (Corrtest CS350). The CV experiments were carried out between 2.0 and 4.5 V at a scan rate of 0.1 mV s^{-1}, and the frequency range of the EIS was 10^5–10^{-3} Hz at a potentiostatic signal amplitude of 5 mV.

Results and discussion

Structure and morphology characterizations

The synthesized samples were characterized by XRD measurements. Figure 1 shows the powder XRD patterns of the $Fe_{(1-x)}Co_xF_3$/MWCNT composites ($x = 0$, 0.02, 0.04 and 0.06), which are in good agreement with those of FeF_3 (JCPDS no. 33-0647), in line with previously reported results [9, 18, 21]. It is noticed that the XRD pattern of FeF_3 shows the distinct diffraction peaks positioned at $2\theta = 24.1°$, 48.2° and 54.3°, which correspond to (012), (024) and (116)

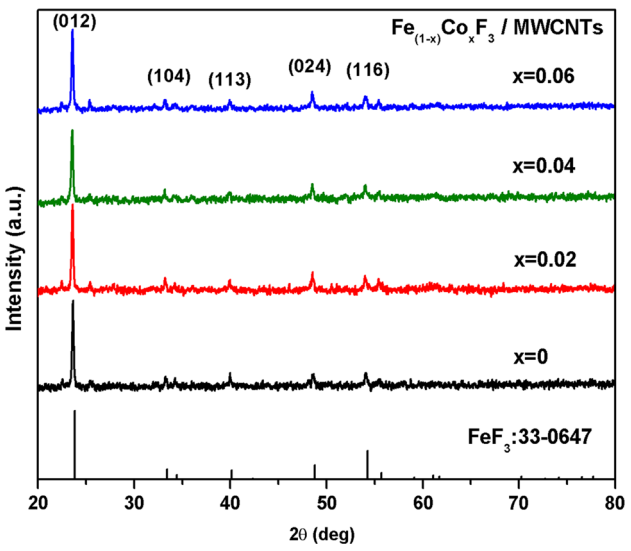

Figure 1 XRD patterns of the standard card of FeF_3 and the $Fe_{(1-x)}Co_xF_3$/MWCNT composites with different Co contents ($x = 0$, 0.02, 0.04 and 0.06).

diffraction peaks of FeF_3. Additionally, there are no MWCNT (carbon) signals detected due to its amorphous structure. Table 1 shows the lattice constants of the $Fe_{(1-x)}Co_xF_3$/MWCNTs ($x = 0$, 0.02, 0.04 and 0.06). It is observed that the values of a, b and c become little smaller or bigger, while those of the volume become slightly smaller after Co-doping. It is found that the radius of Fe^{3+} (0.067 nm) is larger than of Co^{3+} (0.065 nm), which is possible for Co to occupy the Fe site [19]. As shown by the powder XRD patterns in Fig. 1 ($x = 0.02$, $x = 0.04$ and $x = 0.06$), Co-doping led to only a slight inhomogeneous lattice distortion, but did not significantly influence the FeF_3 crystal structure.

The morphologies of the $Fe_{(1-x)}Co_xF_3$/MWCNT composites ($x = 0$, 0.02, 0.04 and 0.06) were characterized by SEM (before and after ball milling). Figure 2a-d shows the SEM images of the FeF_3 and $Fe_{(1-x)}Co_xF_3$/MWCNT samples ($x = 0$, 0.02, 0.04 and 0.06) before ball milling. Obviously, the particle sizes with rectangular shapes have average lengths of 8 μm, and the tiny particles attached in the rectangular particles increase with the increasing Co-dopant amount, which can improve the electrolyte permeation and electrochemical performance [18, 22, 23]. Besides, the morphologies of the $Fe_{(1-x)}Co_xF_3$/MWCNT nanocomposites, which were obtained by ball milling with different Co contents and a constant MWCNT content, are revealed by the SEM images (Fig. 2e–h).

After ball milling for 3 h, the morphologies of the as-prepared $Fe_{(1-x)}Co_xF_3$/MWCNT composites have been changed from rectangular to particles with no visible crystal shape and agglomerating on some level. The particle sizes are reduced to nanoscale (50–200 nm). The MWCNTs are separated into individual carbon nanotubes that reduce the sizes of the interconnected particles, increase the number of nucleation sites and enhance the electronic conductivities [24]. Compared with Fig. 2e–h, the $Fe_{0.96}Co_{0.04}F_3$/MWCNTs (Fig. 2g) exhibit better electrochemical performance due to the minimum amount of agglomeration.

Based on the SEM images in Fig. 3a, EDS elemental mapping was employed to identify the distribution of Fe (Fig. 3b) and Co (Fig. 3c). It is found that Co and Fe are uniformly distributed in the interior space of the $Fe_{0.96}Co_{0.04}F_3$ material. Additionally, EDS (see Fig. 3d) illustrates that the samples contain Fe, Co, F and O (the Cu signal comes from the loading

Table 1 Lattice constants analyzed by the XRD

Samples	a (Å)	b (Å)	c (Å)	Volume (Å^3)
FeF_3/MWCNTs	5.2465	5.2465	13.1632	362.3271
$Fe_{0.98}Co_{0.02}F_3$/MWCNTs	5.2385	5.2385	13.1601	361.1379
$Fe_{0.96}Co_{0.04}F_3$/MWCNTs	5.2432	5.2432	13.1618	361.8329
$Fe_{0.94}Co_{0.06}F_3$/MWCNTs	5.2327	5.2327	13.1705	360.6234

substrate), and no other foreign elements are involved within the whole process.

In order to further accurately observe the morphologies of the $Fe_{0.96}Co_{0.04}F_3$/MWCNT nanocomposites, high-resolution transmission electron microscopy (HRTEM) and selected area electron diffraction (SAED) images are shown in Fig. 4. It can be clearly seen that the crystalline regions of $Fe_{0.96}Co_{0.04}F_3$ and the MWCNTs coexist in the $Fe_{0.96}Co_{0.04}F_3$/MWCNT nanocomposites. In addition, the surfaces of the nanoparticles were fully wrapped by the MWCNT network, which can be beneficial to electron and ion transfer to reduce polarization [25], as shown in Fig. 4a. Figure 4b, c shows the HRTEM of the $Fe_{0.96}Co_{0.04}F_3$/MWCNT nanocomposites. It is noticed that well-crystallized regions and tube-shaped regions coexist in the $Fe_{0.96}Co_{0.04}F_3$/MWCNT nanocomposites. The discrete spots of the SAED pattern of $Fe_{0.96}Co_{0.04}F_3$/MWCNT nanocomposites in Fig. 4d indicate the (012), (024) and (224) planes, and broad ring patterns exist together, which is consistent with XRD results. The SEM and TEM images confirm that the morphology of the $Fe_{0.96}Co_{0.04}F_3$/MWCNTs is consistent with our goals. The $Fe_{0.96}Co_{0.04}F_3$/MWCNT nanocomposites exhibit a high specific surface area, which is beneficial for enhancing charge transfer reactions and the electrode/electrolyte contact area. Meanwhile, the specific contact morphology can reduce the diffusion distance of Li^+. Therefore, the samples are expected to display good rate performances and cycling stabilities.

Electrochemical characterization

Electrochemical characterization of the FeF_3/MWCNTs

In order to investigate the effect of in situ wrapping MWCNTs, the galvanostatic charge–discharge profiles of the FeF_3/MWCNT nanocomposite cathodes were tested within a voltage window from 2.0 to 4.5 V at 0.2 C (1 C = 237 mA g^{-1}; the weight ratio of MWCNTs is $\omega_1 = 1\%$, $\omega_2 = 3\%$ and $\omega_3 = 5\%$, respectively), as shown in Fig. 5. The initial discharge capacities of the FeF_3/MWCNT electrodes with $\omega_1 = 1\%$, $\omega_2 = 3\%$ and $\omega_3 = 5\%$ are 179.4, 192.1 and 172.1 mAh g^{-1}, respectively, as shown in Fig. 5a. It is notable that the FeF_3/MWCNT electrodes are first discharged before charge. After 50 cycles, the discharge capacities of the FeF_3/MWCNT nanocomposites (Fig. 5b) faded to 153.8 160.7 and 146.6 mAh g^{-1}, respectively, which demonstrates that adding ω_2 of the MWCNTs effectively improved the specific capacity of FeF_3. Moreover, in situ wrapping of the MWCNTs could form conductive networks on the surface of the FeF_3 nanoparticles, which is expected to enhance the conductivity of the samples and improve their electrochemical performances [22, 26]. However, excessive MWCNTs will inhibit the initial efficiency due to its large specific surface area. Therefore, we can investigate Co-dopant of FeF_3 by selecting the optimal MWCNT amount ($\omega_2 = 3\%$).

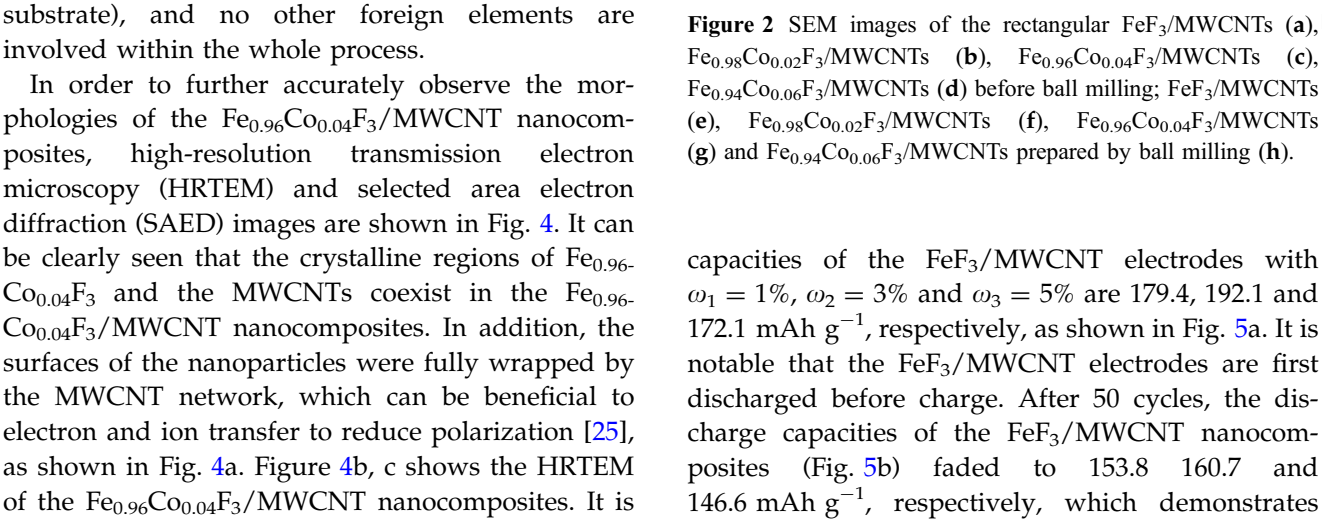

Figure 2 SEM images of the rectangular FeF_3/MWCNTs (**a**), $Fe_{0.98}Co_{0.02}F_3$/MWCNTs (**b**), $Fe_{0.96}Co_{0.04}F_3$/MWCNTs (**c**), $Fe_{0.94}Co_{0.06}F_3$/MWCNTs (**d**) before ball milling; FeF_3/MWCNTs (**e**), $Fe_{0.98}Co_{0.02}F_3$/MWCNTs (**f**), $Fe_{0.96}Co_{0.04}F_3$/MWCNTs (**g**) and $Fe_{0.94}Co_{0.06}F_3$/MWCNTs prepared by ball milling (**h**).

Electrochemical characterization of $Fe_{(1-x)}Co_xF_3$/MWCNTs

The $Fe_{(1-x)}Co_xF_3$/MWCNT nanocomposites ($x = 0$, 0.02, 0.04 and 0.06) were composed of MWCNTs ($\omega_2 = 3\%$) and $Fe_{(1-x)}Co_xF_3$, prepared using the in situ solvothermal method. Figure 6a shows the initial discharge and charge profiles of the $Fe_{(1-x)}Co_xF_3$/MWCNT nanocomposites ($x = 0$, 0.02, 0.04 and 0.06) at a current density of 0.2 C in the voltage range of 2.0–4.5 V. The initial discharge capacities of 192.1, 206.8, 217.0 and 199.1 mAh g^{-1} were obtained for Co-doping levels of $x = 0$, 0.02, 0.04 and 0.06, respectively. Additionally, after 50 cycles (Fig. 6b), the discharge capacities of the FeF_3/MWCNTs,

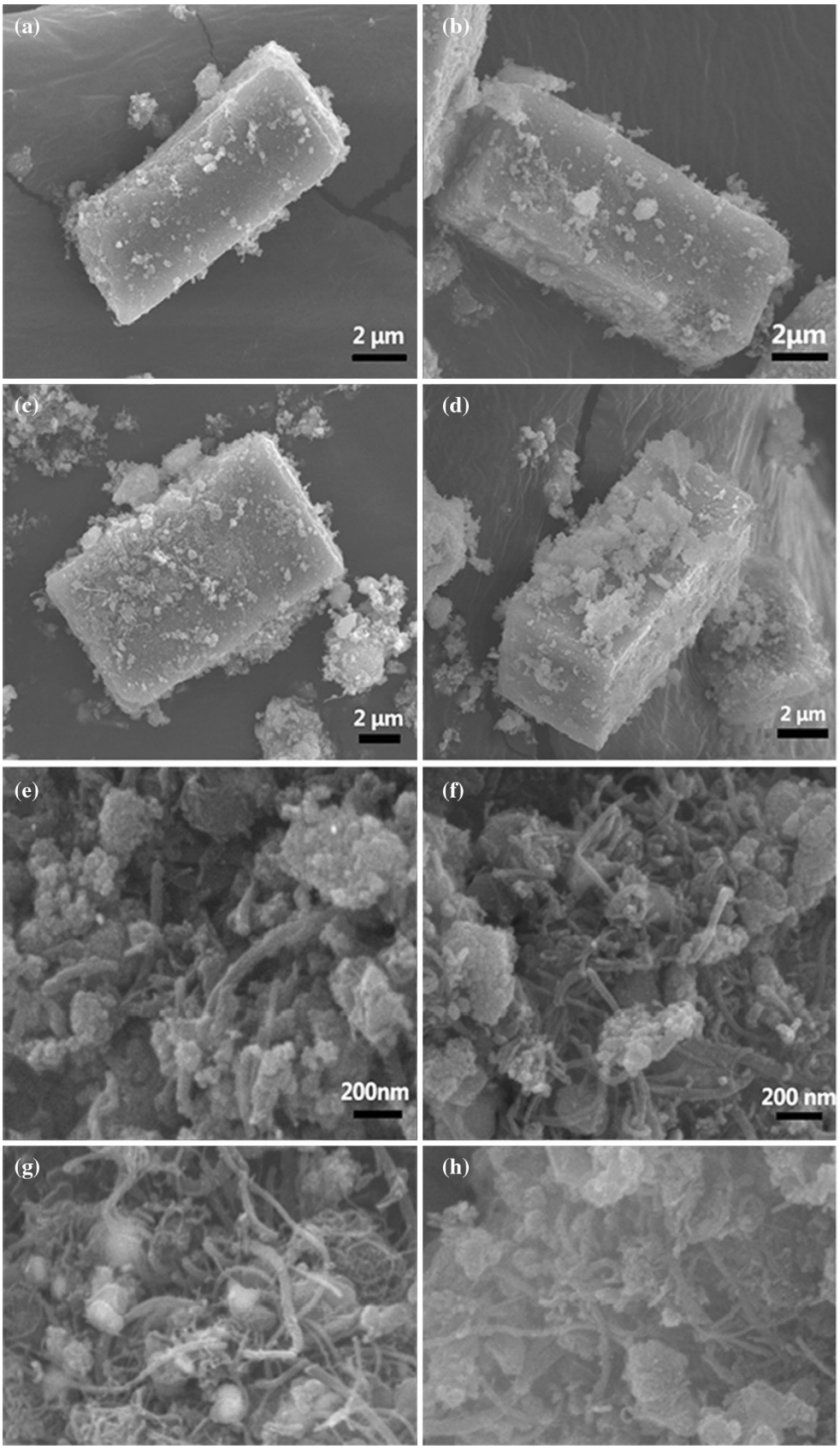
(a)
2 µm
(b)
2µm
(c)
2 µm
(d)
2 µm
(e)
200nm
(f)
200 nm
(g)
(h)

$Fe_{0.98}Co_{0.02}F_3$/MWCNTs, $Fe_{0.96}Co_{0.04}F_3$/MWCNTs and $Fe_{0.94}Co_{0.06}F_3$/MWCNTs were 160.7, 177.8, 187.9 and 170.5 mAh g^{-1}, respectively. It is clear that the $Fe_{(1-x)}Co_xF_3$/MWCNT nanocomposites exhibit sloped reaction plateaus of 2.7 V. Obviously, the Co-doped FeF_3/MWCNT nanocomposites show better electrochemical properties than pristine FeF_3/MWCNTs. In addition, the $Fe_{0.96}Co_{0.04}F_3$/MWCNT nanocomposite exhibited the highest discharge voltage plateau and the highest specific capacity, which suggests that this composite possesses the smallest electrochemical polarization due to efficient Li^+ transport [13, 18].

To further test the cycling performances of the Co-doped composites, the cycling performances of $Fe_{(1-x)}Co_xF_3$/MWCNTs at 0.2 and 3 C in the voltage range of 2.0–4.5 V over 50 cycles are shown in Fig. 6c, d. It is notable that the coulombic efficiencies of Co-doped materials are as high as 97% and obviously higher than those of pure FeF_3/MWCNTs at 0.2 and 3 C during 50 cycles. As seen from the voltage profiles, the capacity retentions of the $Fe_{0.96}Co_{0.04}F_3$/MWCNT electrode were 92.7% at 0.2 C and 90.1% at 3 C. Similarly, the FeF_3/MWCNT electrode displayed capacity retentions of 88.6% at 0.2 C and 79.1% at 3 C; the $Fe_{0.98}Co_{0.02}F_3$/MWCNT electrode displayed 90.2% at 0.2 C and 86.4% at 3 C; the $Fe_{0.94}Co_{0.06}F_3$/MWCNT electrode displayed 89.7% at 0.2 C and 84.1% at 3 C. Thus, the Co-doped samples also showed significantly better cycling stabilities than the undoped sample at 3 C. In addition, the $Fe_{0.96}Co_{0.04}F_3$/MWCNT electrode exhibited the highest capacity retention.

In order to detect the electrochemical performances after Co-doping, CV measurements of the $Fe_{(1-x)}Co_xF_3$/MWCNT nanocomposites ($x = 0$, 0.02, 0.04 and 0.06) were compared, as shown in Fig. 7a. The CV curves of the $Fe_{(1-x)}Co_xF_3$/MWCNT cathodes were collected at a scan rate of 0.1 mV s^{-1} between 2.0 and 4.5 V. The four curves exhibit similar shapes with a pair of reversible reduction and oxidation peaks corresponding to the insertion/extraction of Li^+, indicating that these samples have similar

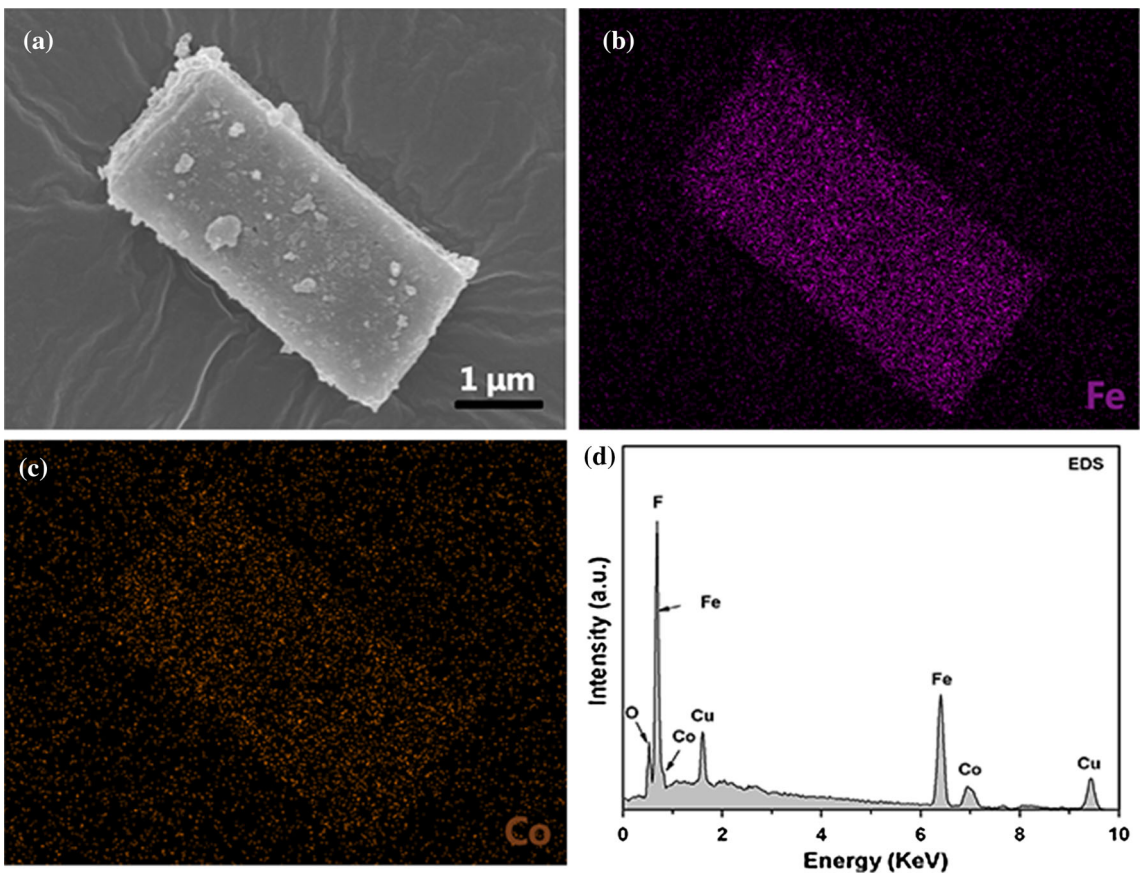

Figure 3 EDS elemental mapping images of the $Fe_{0.96}Co_{0.04}F_3$ composite: SEM image of the mapping area (**a**), Fe (**b**) and Co (**c**); the EDS spectrum showing strong Fe, Co, F and O signals (**d**).

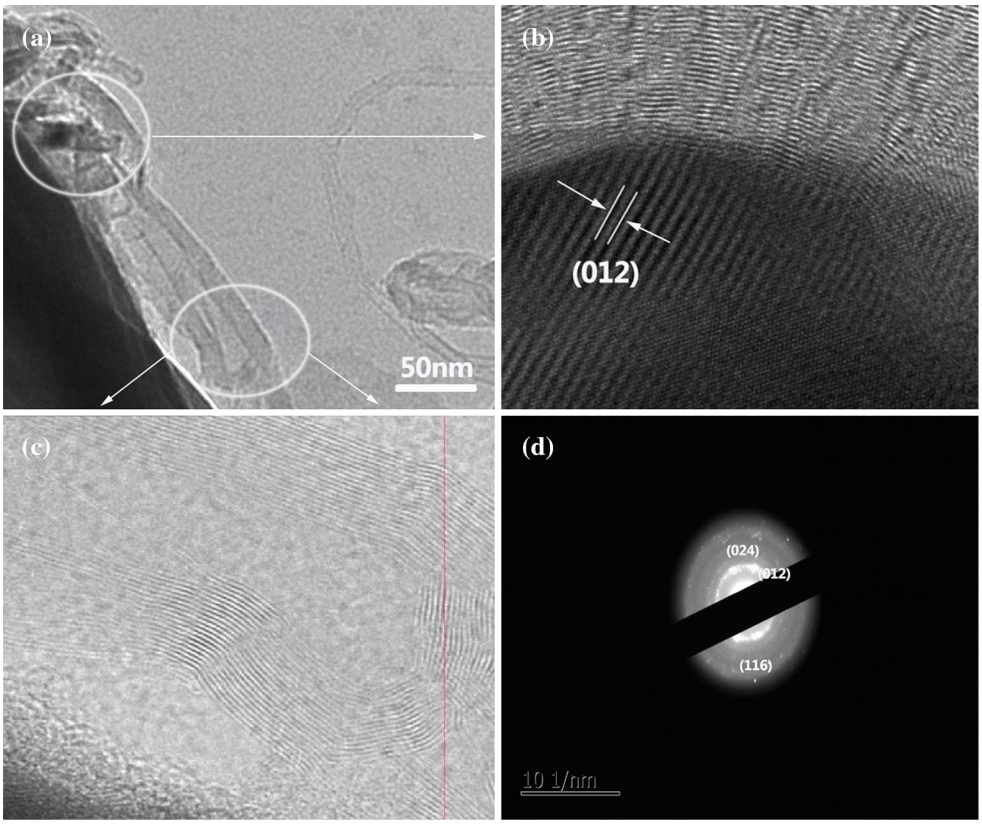

Figure 4 TEM image of $Fe_{0.96}Co_{0.04}F_3$/MWCNTs (**a**); HRTEM image of the $Fe_{0.96}Co_{0.04}F_3$/MWCNT nanoparticle (**b**) and (**c**); SEAD patterns of $Fe_{0.96}Co_{0.04}F_3$/MWCNTs (**d**).

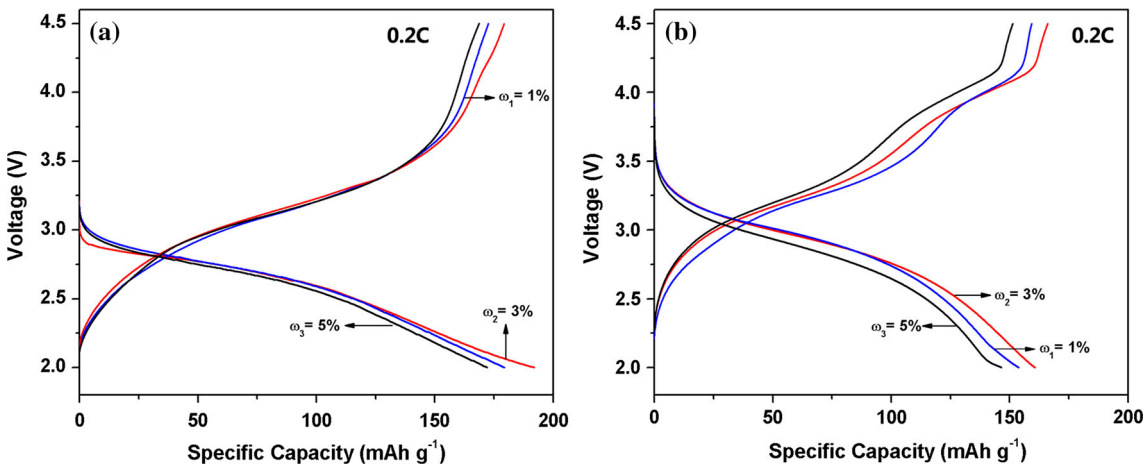

Figure 5 **a** Initial cycle and **b** the 50th cycle charge/discharge curves of the FeF_3/MWCNT nanocomposites ($\omega_1 = 1\%$, $\omega_2 = 3\%$ and $\omega_3 = 5\%$) at a rate of 0.2 C (1 C = 237 mA g^{-1}) in the voltage range of 2.0–4.5 V.

electrochemical reaction mechanisms. However, the $Fe_{(1-x)}Co_xF_3$/MWCNT nanocomposites ($x = 0.02, 0.04$ and 0.06) have significantly smaller differences between their cathodic and anodic peaks, with ΔE values of 0.30, 0.24 and 0.32 V, respectively, compared to those of FeF_3/MWCNTs (0.43 V). Thus, the FeF_3/MWCNT nanocomposite showed th highest polarization. Additionally, $Fe_{0.96}Co_{0.04}F_3$/MWCNTs ($\Delta E = 0.24$ V) showed a higher current and larger area of the CV curve, which are directly related to the achieved capacity. These results demonstrate that Co-doping can improve the

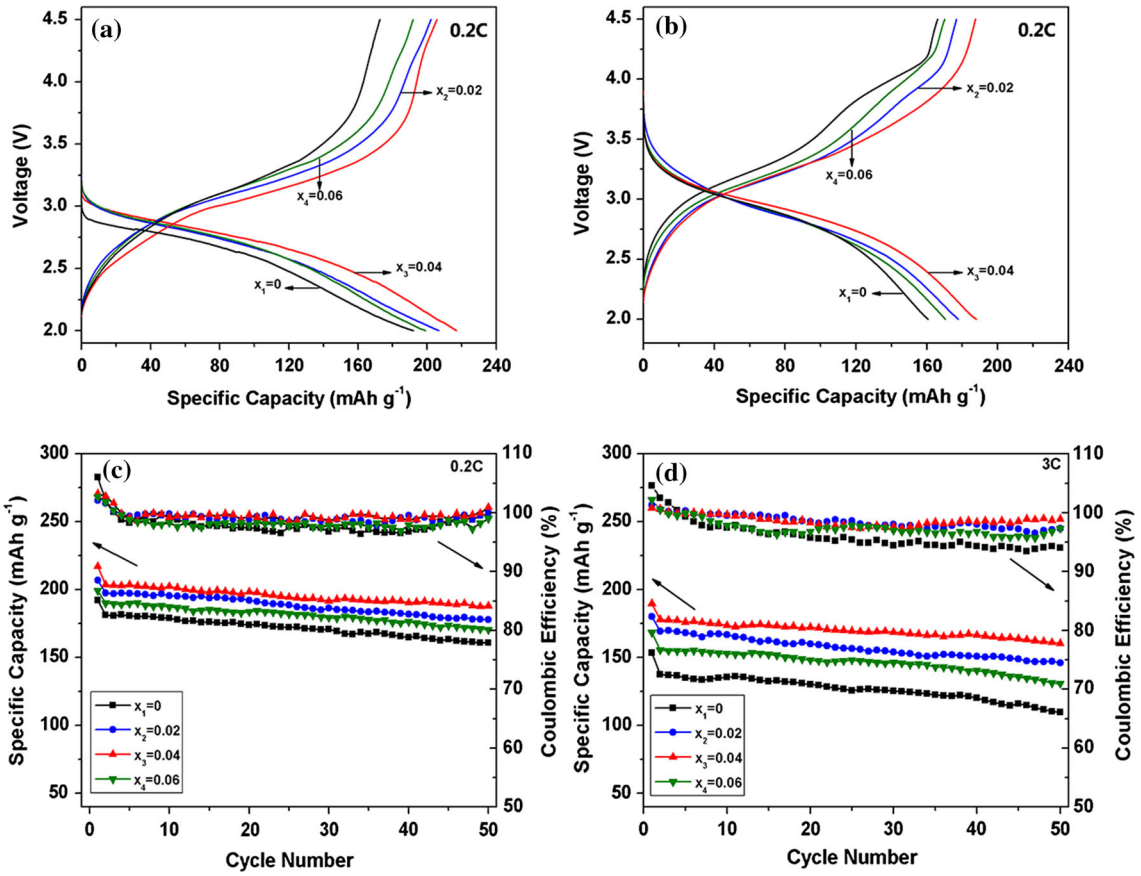

Figure 6 Initial cycle (**a**) and the 50th cycle (**b**) charge/discharge curves of the $Fe_{(1-x)}Co_xF_3$/MWCNT nanocomposite ($x = 0$, 0.02, 0.04 and 0.06) electrodes at a rate of 0.2 C in the voltage range of 2.0–4.5 V; cycling performances of the samples at 0.2 C (**c**) and 3 C (**d**).

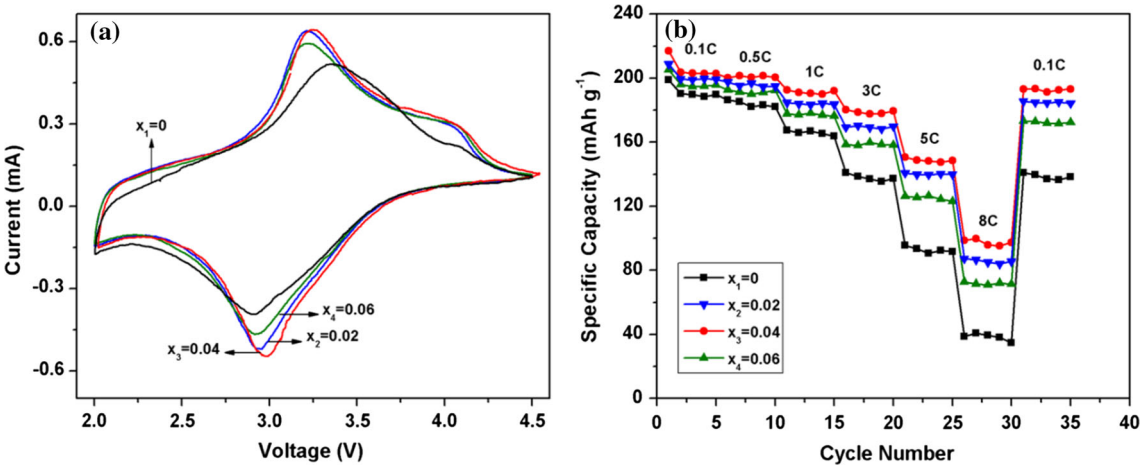

Figure 7 **a** CV curves of the $Fe_{(1-x)}Co_xF_3$/MWCNT nanocomposites ($x = 0$, 0.02, 0.04 and 0.06) at 0.2 C in the voltage range of 2.0–4.5 V (the scan rate of CV curves is 0.1 mV s^{-1}); **b** rate performance of the $Fe_{(1-x)}Co_xF_3$/MWCNT nanocomposites ($x = 0$, 0.02, 0.04 and 0.06) at various current densities.

electrochemical performance of FeF_3/MWCNTs, in complete agreement with the improvements in both the cycling and charge–discharge performances of the $Fe_{0.96}Co_{0.04}F_3$/MWCNT sample shown in Fig. 6.

To assess the rate performance of the $Fe_{(1-x)}Co_xF_3$/MWCNT nanocomposites, the rate performance curves shown in Fig. 7b were generated at various current densities from 0.1 to 8 C and finally back to

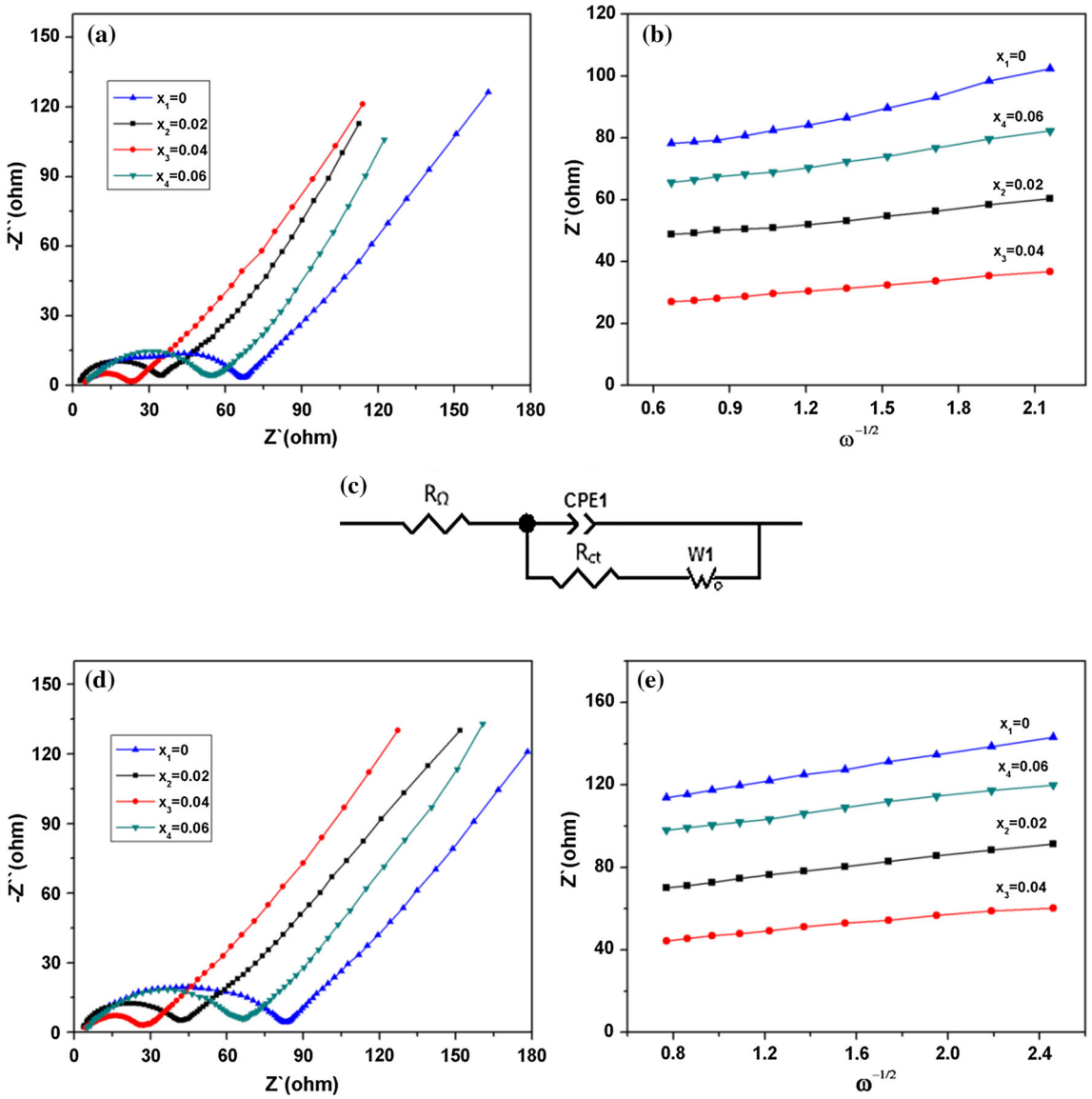

Figure 8 EIS analysis of the $Fe_{(1-x)}Co_xF_3$/MWCNT electrodes ($x = 0$, 0.02, 0.04 and 0.06) after the first (**a**) and 50th (**d**) cycles; the relationship of the first (**b**) and 50th (**e**) cycles between Z' and $\omega^{-1/2}$ in the low-frequency region; **c** the equivalent circuit model.

0.1 C. As the current density is increased, the discharge capacities of the samples decrease. The capacity retentions of the $Fe_{(1-x)}Co_xF_3$/MWCNT nanocomposites ($x = 0$, 0.02, 0.04 and 0.06) were 72.8, 91.8, 94.9 and 88.5%, respectively. Interestingly, the $Fe_{(1-x)}Co_xF_3$/MWCNTs ($x = 0.02$, 0.04 and 0.06) showed significantly enhanced rate capabilities and capacity retentions compared to the FeF_3/MWCNTs. Moreover, these results indicate that the $Fe_{0.96}Co_{0.04}F_3$/MWCNT sample exhibits higher structural stability and reversibility than the other samples.

Figure 8a, d shows the EIS curves of the $Fe_{(1-x)}Co_xF_3$/MWCNT nanocomposites after the first and 50th cycles at room temperature. Each curve is composed of a semicircle in the high-frequency region and a line in the low-frequency region. An equivalent circuit model was used to analyze the impedance spectra, as shown in Fig. 8c, where R_Ω is the electrolyte resistance, R_{ct} is the Li^+ charge transfer resistance at the interface and CPE_1 is the constant phase element, which was used to represent the double-layer capacitance and the passivation film capacitance. The slope of the line in the low-frequency region represents the Warburg impedance (W_1), which is attributed to the diffusion of Li^+ into the electrode. It is clear that in all the curves the R_Ω

Table 2 Values of σ, R_Ω, R_{ct} and D_{Li+} for the $Fe_{(1-x)}Co_xF_3$/MWCNT samples after different cycles

$Fe_{(1-x)}Co_xF_3$/MWCNTs	First			50th		
	σ	R_{ct} (Ω)	D_{Li+} ($cm^2\ s^{-1}$)	σ	R_{ct} (Ω)	D_{Li+} ($cm^2\ s^{-1}$)
$x_1 = 0$	9.45	70.80	8.06×10^{-12}	10.56	85.36	6.45×10^{-12}
$x_2 = 0.02$	8.04	38.57	1.09×10^{-11}	8.82	47.62	9.10×10^{-12}
$x_3 = 0.04$	6.45	23.89	1.72×10^{-11}	7.15	31.25	1.40×10^{-11}
$x_4 = 0.06$	8.51	56.12	9.73×10^{-12}	9.36	67.37	8.05×10^{-12}

values (~3 Ω) are almost same due to the same electrolyte. Interestingly, the R_{ct} value of the $Fe_{(1-x)}Co_xF_3$/MWCNT electrodes ($x = 0.02$, 0.04 and 0.06) is smaller than that of FeF_3/MWCNTs after the first and 50th cycles, as shown in Table 2. Therefore, the low total resistance of the Co-doped FeF_3/MWCNT nanocomposite indicates a higher conductivity and less polarization than of FeF_3/MWCNTs which are in favor of the transmission of ions and thus improve cycling and rate performance. In order to calculate the influence of Co-doping on the diffusion of Li^+, the following formula was utilized [18]:

$$D_{Li+} = \frac{R^2T^2}{2n^4A^2F^4C^2\sigma^2} \quad (1)$$

In Eq. (1), T is temperature (room temperature in our experiments, 298 K); R is the ideal gas constant (8.314 $JK^{-1}\ mol^{-1}$); n is the number of the electrons per molecule during the electronic transfer reaction; A is the surface area of the electrode; F is the Faraday constant (96500 C mol^{-1}); C is the molar concentration of Li^+ in the $Fe_{(1-x)}Co_xF_3$ electrode; and σ is the Warburg factor, which has the following relationship with Z' [27]:

$$Z' = \sigma\omega^{-1/2} + R_\Omega + R_{ct} \quad (2)$$

Here, ω is the frequency in the low-frequency region, and the slope of line of $Z' \sim \omega^{-1/2}$ [28] is obtained as shown in Fig. 8b, e. The parameters of the equivalent circuit obtained by computer simulations are shown in Table 2, which were calculated based on Eqs. (1) and (2). Figure 8b implies the Li^+ diffusion coefficients of $Fe_{(1-x)}Co_xF_3$/MWCNT electrodes after the first cycle. The calculated Li^+ diffusion coefficients of the $Fe_{(1-x)}Co_xF_3$/MWCNT electrodes are 8.06×10^{-12}, 1.09×10^{-11}, 1.72×10^{-11} and 9.73×10^{-12} $cm^2\ s^{-1}$, respectively, indicating that the $Fe_{0.96}Co_{0.04}F_3$/MWCNT nanocomposite exhibits the highest Li^+ diffusion coefficient. Similarly, $Fe_{0.96}Co_{0.04}F_3$/MWCNT electrode at 50th cycles exhibited the highest Li^+ diffusion coefficient ($D_{Li+} = 1.40 \times 10^{-11}$ $cm^2\ s^{-1}$) compared to that of other electrodes according to investigation. Obviously, the Li^+ diffusion coefficient was improved after Co-doping, which implies that a larger Li^+ diffusion coefficient results in an electrode with a higher capacity during charging and discharging. A less significant increase in impedance during cycling indicates a lower polarization, which results in good cycling behavior. We found that a suitable Co-doping concentration can improve the electrochemical performance of FeF_3/MWCNTs. However, the experimental data analysis shows that the crystal growth of Co-dopant also restrains Li^+ diffusion and increases surface impedance, which is contradicted to the result of decreasing band gap. These results fully demonstrate the above conclusions of the CV and cycling tests.

Conclusions

In summary, $Fe_{(1-x)}Co_xF_3$/MWCNT nanocomposites ($x = 0$, 0.02, 0.04 and 0.06) were successfully fabricated by an in situ solvothermal method. The MWCNTs ($\omega_2 = 3\%$) were firmly bonded to the $Fe_{(1-x)}Co_xF_3$ materials to provide electron transfer pathways, which were able to enhance the conductivity and reduce the sizes of the interconnected particles of the $Fe_{(1-x)}Co_xF_3$ materials. The CV measurement results show that the Co-doped could improve the dynamic behavior. The EIS indicates that the Co-doped greatly enhances the charge transfer resistance of FeF_3/MWCNTs. Our analyses demonstrated that Co-doping can adjust the crystal structure, reduce the polarization and improve the Li^+ diffusion coefficient of FeF_3. However, the overgrowth of Co-dopant will restrain Li^+ diffusion and increase surface impedance, which has an opposite effect with the result of decreasing band gap. In order to solve the issue of the microcrystal growth and the band gap reduction, a kind of suitable Co-doping concentration is selected.

Consequently, the $Fe_{0.96}Co_{0.04}F_3$/MWCNT nanocomposite exhibited the highest specific capacity, cycling stability and rate performance. The initial discharge specific capacity of the $Fe_{0.96}Co_{0.04}F_3$/MWCNT nanocomposite reached 217.0 mAh g^{-1} at 0.2 C. After 50 cycles, the discharge specific capacity was maintained at 187.9 mAh g^{-1}. Meanwhile, the capacity retention remains 89.7% at a rate of 3 C after 50 cycles. The EIS results revealed that both the Li^+ charge transfer resistance ($R_{ct} = 31.25\ \Omega$) and Li^+ diffusion coefficient (1.40×10^{-11} cm^2 s^{-1}) were satisfactory from Co-doping and the in situ wrapping of the MWCNTs after the 50th cycle. This study demonstrated that the in situ wrapping of the MWCNTs and Co-doping are effective methods to enhance the electrochemical performance of FeF_3. Therefore, the $Fe_{(1-x)}Co_xF_3$/MWCNT electrodes are a potential cathode material for LIBs.

Acknowledgements

This work is supported by Science and Technology Plan Foundation of Guangdong (2015A050502046) and Science and Technology Plan Foundation of Guangzhou (201704030031).

References

[1] Bruce PG (2008) Energy storage beyond the horizon: rechargeable lithium batteries. Solid State Ion 179:752–760

[2] Armand M, Tarascon JM (2008) Building better batteries. Nature 451:652–657

[3] Li H, Balaya P, Maier J (2004) Li-storage via heterogeneous reaction in selected binary metal fluorides and oxides. J Electrochem Soc 151:A1878–A1885

[4] Zhou MJ, Zhao LW, Okada S, Yamaki JI (2011) Thermal characteristics of a FeF_3 cathode via conversion reaction in comparison with $LiFePO_4$. J Power Sources 196:8110–8115

[5] Li L, Meng F, Jin S (2012) High-capacity lithium-ion battery conversion cathodes based on iron fluoride nanowires and insights into the conversion mechanism. Nano Lett 12:6030–6037

[6] Jiang J, Li LP, Xu MW, Zhu JH, Ming C (2016) FeF_3@thin nickel ammine nitrate matrix: smart configurations and applications as superior cathodes for Li-ion batteries. ACS Appl Mater Interfaces 8:16240–16247

[7] Ma R, Lu Z, Wang C, Wang H, Yang S, Xi L, Chung J (2013) Large-scale fabrication of graphene-wrapped FeF_3 nanocrystals as cathode materials for lithium ion batteries. Nanoscale 5:6338–6343

[8] Li CL, Gu L, Tong JW, Tsukimoto S (2011) A mesoporous iron-based fluoride cathode of tunnel structure for rechargeable lithium batteries. Adv Funct Mater 21:1391–1397

[9] Jangwook L, Byoungwoo K (2016) Novel and scalable solid-state synthesis of a nanocrystalline FeF_3/C composite and its excellent electrochemical performance. Chem Commun 52:9414–9417

[10] Li CL, Gu L, Tong JW, Maier J (2011) Carbon nanotu be wiring of electrodes for high-rate lithium batteries using an imidazolium-based ionic liquid precursor as dispersant and binder: a case study on iron fluoride nanoparticles. ACS Nano 5:2930–2938

[11] Ma DL, Wang HG, Li Y, Xu D, Yuan S, Huang XL, Zhang XB, Zhang Y (2014) In situ generated FeF_3 in homogeneous iron matrix toward high-performance cathode material for sodium-ion batteries. Nano Energy 10:295–304

[12] Chu QX, Xing ZC, Ren XB, Asiri AM, Al-youbi AO, Alamry KA, Sun XP (2013) Reduced graphene oxide decorated with FeF_3 nanoparticles: facile synthesis and application as a high capacity cathode material for rechargeable lithium batteries. Electrochim Acta 111:80–85

[13] Wu W, Wang Y, Wang XY, Chen QQ, Wang X, Yang SY, Liu XM (2009) Structure and electrochemical performance of FeF_3/V_2O_5 composite cathode material for lithium-ion battery. J Alloy Compd 486:93–96

[14] Xu XP, Chen S, Shui M, Xu LX, Zheng WD, Shu J, Cheng LL, Feng L, Ren YL (2014) One step solid state synthesis of $FeF_3{\cdot}0.33H_2O$/C nano-composite as cathode material for lithium-ion batteries. Ceram Int 40:3145–3148

[15] Fan LH, Li BJ, Zhang NQ, Sun KN (2015) Carbon nanohorns carried iron fluoride nanocomposite with ultrahigh rate lithium ion storage properties. Sci Rep 5:12154–12162

[16] Li CL, Yin CL, Gu L, Dinnebier RE (2013) An $FeF_3{\cdot}0.5H_2O$ polytype: a microporous framework compound with intersecting tunnels for Li and Na batteries. J Am Chem Soc 135:11425–11428

[17] Li H, Richter G, Maier J (2003) Reversible formation and decomposition of LiF clusters using transition metal fluorides as precursors and their application in rechargeable Li batteries. Adv Mater 15:736–739

[18] Bai Y, Zhou XZ, Jia Z, Wu C, Yang LW, Chen MZ, Zhao H, Wu F, Liu G (2015) Understanding the combine effects of microcrystal growth and band gap reduction for $Fe_{(1-x)}Ti_xF_3$ nanocomposites as cathode materials for lithium-ion batteries. Nano Energy 17:140–151

[19] Liu L, Zhou M, Yi LH, Guo HP, Tan JL, Shu HB, Yang XK, Yang ZH, Wang XY (2012) Excellent cycle performance of

Co-doped FeF_3/C nanocomposite cathode material for lithium-ion batteries. J Mater Chem 22:17539–17550

[20] Yang ZH, Pei Y, Wang XY, Liu L, Su X (2012) First principles study on the structural, magnetic and electronic properties of Co-doped FeF_3. Comput Theor Chem 1:44–48

[21] Jung H, Shin J, Chae CJK, Lee J Lim (2013) FeF_3/ordered mesoporous carbon (OMC) nanocomposites for lithium ion batteries with enhanced electrochemical performance. J Phys Chem C 117:14939–14946

[22] An HF, Wang Y, Wang XY, Zheng LP, Wang XY, Yi LH, Bai L, Zhang XY (2010) Polypyrrole/carbon aerogel composite materials for supercapacitor. J Power Sources 195:6964–6969

[23] Cho J, Kim H, Park B (2004) Comparison of overcharge behavior of $AlPO_4$-coated $LiCoO_2$ and $LiNi_{0.8}Co_{0.1}Mn_{0.1}O_2$ cathode materials in Li-ion cells. J Electrochem Soc 151:A1707–A1711

[24] Wei SY, Wang XY, Zhang R, Hu H, Shen YQ, Liu J (2016) Preparation and performance of spherical $FeF_{2.5}{\cdot}0.5H_2O$ nanoparticles wrapped by MWCNTs as cathode material of lithium ion batteries. RSC Adv 6:97759–97769

[25] Lu Y, Wen ZY, Jin J, Rui K, Wu XW (2014) Hierarchical mesoporous iron-based fluoride with partially hollow structure: facile preparation and high performance as cathode material for rechargeable lithium ion batteries. Phys Chem Chem Phys 16:8556–8562

[26] Fukushima T, Kosaka A, Ishimura Y, Yamamoto T, Takigawa T, Ishii N, Aida T (2003) Molecular ordering of organic molten salts triggered by single-walled carbon nanotube. Science 300:2072–2074

[27] Gao F, Tang ZY (2008) Kinetic behavior of $LiFePO_4$/C cathode material for lithium-ion batteries. Electrochim Acta 53:5071–5075

[28] Wang XY, Hao H, Liu JL, Huang T, Yu AS (2011) A novel method for preparation of macroposous lithium nickel manganese oxygen as cathode material for lithium ion batteries. Electrochim Acta 56:4065–4069